J|A|C|S
ARTICLES

Controlled-Access Hollow Mechanized Silica Nanocontainers

Li Du,[†,‡] Shijun Liao,[*,‡] Hussam A. Khatib,[§] J. Fraser Stoddart,[*,§] and
Jeffrey I. Zink[*,†]

*Department of Chemistry and Biochemistry, University of California, Los Angeles, California
90095, School of Chemistry and Chemical Engineering, South China University of Technology,
Guangzhou, China 510640, and Department of Chemistry, Northwestern University,
Evanston, Illinois 60208*

Received June 17, 2009; E-mail: zink@chem.ucla.edu; stoddart@northwestern.edu; chsjliao@scut.edu.cn

Abstract: A new category of mechanized nanoparticles, consisting of a hollow mesoporous silica spherical framework controlled by a supramolecular system containing the α-cyclodextrin (α-CD) ring on a stalk that is tethered to the pore openings on the nanosphere, is synthesized and tested. Construction of the nanovalve relies on the hydrogen-bonding interaction between α-CD and the stalk. The stalk is bonded to the nanoparticle chemically and contains an anilino group that is located on the end of the linker molecule that is closest to the pore entrance. When the α-CD ring is complexed with the stalk at neutral pH, the bulky cyclic component is located near the pore openings, thereby blocking departure of cargo molecules that were loaded in the nanopores and hollow interior of the particle. Protonation of the nitrogen atoms at lower pH causes the binding affinity to decrease, releasing the α-CD and allowing the cargo molecules to escape. The properties of this newly designed pH-responsive nanovalve are compared to those of conventional mesoporous silica nanoparticles. The on-command pH-activated release is measured using luminescence spectroscopy. The effect of different stalk lengths and pH conditions on the release of fluorescent dye cargo molecules is measured.

Introduction

Functionalized inorganic nanoparticles are attracting increasing interest for drug delivery applications. The two major strategies involve immobilizing the drug molecules on the surface of solid nonporous particles, frequently by using adsorbed or tethered polymers,[1] and most recently by utilizing the interior porosity of mesoporous silica nanoparticles.[2] The latter offers superior carrying capacity and, most importantly, the ability to trap and release molecules physically on command by using a variety of capping agents.[3] A newer type of inorganic nanoparticle consisting of silica with a hollow core has recently been reported;[4] it could have even higher carrying capacity if

the interior could be controllably filled and emptied. Mesoporous silica walls would offer the same opportunity for functionalization with mechanized (super)molecules[5] to control the pore openings as does conventional mesoporous silica. It is unknown if the pore morphology and entrance structure are amenable to derivatization with and control by mechanized (super)molecules.[5] Hollow particles present an additional challenge; all of the pores that are connected to the hollow interior must be controlled. In conventional particles, absence of control of a

† University of California, Los Angeles.
‡ South China University of Technology.
§ Northwestern University.
(1) (a) Park, C.; Youn, H.; Kim, H.; Noh, T.; Kook, Y. H.; Oh, E. T.; Park, H. J.; Kim, C. *J. Mater. Chem.* **2009**, *19*, 2310–2315. (b) Dhar, S.; Reddy, E. M.; Shiras, A.; Pokharkar, V.; Prasad, B. L. V. *Chem.- Eur. J.* **2008**, *14*, 10244–10250. (c) Oh, K. S.; Kim, R. S.; Lee, J.; Kim, D.; Cho, S. H.; Yuk, S. H. *J. Appl. Polym. Sci.* **2008**, *108*, 3239–3244. (d) Aghdam, A. G.; Vossoughi, M.; Almzadeh, I.; Zeinali, M. *J. Dispersion Sci. Technol.* **2008**, *29*, 1062–1065. (e) Bergen, J. M.; Recum, H. A. V.; Goodman, T. T.; Massey, A. P.; Pun, S. H. *Macromol. Biosci.* **2006**, *6*, 506–516.
(2) (a) Vallet-Regi, M.; Balas, F.; Arcos, D. *Angew. Chem., Int. Ed.* **2007**, *46*, 7548–7558. (b) Han, Y. J.; Stucky, G. D.; Butler, A. *J. Am. Chem. Soc.* **1999**, *121*, 9897–9898. (c) Slowing, I. I.; Trewyn, B. G.; Lin, V. S. Y. *J. Am. Chem. Soc.* **2007**, *129*, 8845–8849. (d) Lai, C. Y.; Trewyn, B. G.; Jeftinija, D. M.; Jeftinija, K.; Xu, S.; Jeftinija, S.; Lin, V. S. Y. *J. Am. Chem. Soc.* **2003**, *125*, 4451–4459. (e) Munoz, B.; Ramila, A.; Perez-Pariente, J.; Diaz, I.; Vallet-Regi, M. *Chem. Mater.* **2003**, *15*, 500–503. (f) Liu, J.; Liong, M.; Zink, J. I.; Tammanoi, F. *Small* **2007**, *3*, 1341–1346. (g) Liong, M.; France, B.; Bradley, K. A.; Zink, J. I. *Adv. Mater.* **2009**, *21*, 1684–1689.

(3) (a) Saha, S.; Leung, K. C. F.; Nguyen, T. D.; Stoddart, J. F.; Zink, J. I. *Adv. Funct. Mater.* **2007**, *17*, 685–693. (b) Mal, N. K.; Fujiwara, M.; Tanaka, Y. *Nature* **2003**, *421*, 350–353. (c) Zhu, Y.; Fujiwara, M. *Angew. Chem., Int. Ed.* **2007**, *46*, 2241–2244. (d) Patel, K.; Angelos, S.; Dichtel, W. R.; Coskun, A.; Yang, Y. W.; Zink, J. I.; Stoddart, J. F. *J. Am. Chem. Soc.* **2008**, *130*, 2382–2383. (e) Angelos, S.; Johansson, E.; Stoddart, J. F.; Zink, J. I. *Adv. Funct. Mater.* **2007**, *17*, 2261–2271. (f) Giri, S.; Trewyn, B. G.; Stellmaker, M. P.; Lin, V. S. Y. *Angew. Chem., Int. Ed.* **2005**, *44*, 5038–5044. (g) Slowing, I.; Trewyn, B. G.; Giri, S.; Lin, V. S. Y. *Adv. Funct. Mater.* **2007**, *17*, 1225–1236. (h) Ferris, D. P.; Zhao, Y.; Khashab, N. M.; Khatib, H. A.; Stoddart, J. F.; Zink, J. I. *J. Am. Chem. Soc.* **2009**, *131*, 1686–1688. (i) Nguyen, T. D.; Leung, K. C. F.; Liong, M.; Pentecost, C. D.; Stoddart, J. F.; Zink, J. I. *Org. Lett.* **2006**, *8*, 3363–3366.
(4) (a) Zhu, Y.; Shi, J.; Li, Y.; Chen, H.; Shen, W.; Dong, X. *J. Mater. Res.* **2005**, *20*, 54–61. (b) Zhao, W. R.; Chen, H. R.; Li, Y. S.; Li, L.; Lang, M. D.; Shi, J. L. *Adv. Funct. Mater.* **2008**, *18*, 2780–2788. (c) Zhu, Y.; Shi, J.; Li, Y.; Chen, H.; Shen, W.; Dong, X. *Microporous Mesoporous Mater.* **2005**, *85*, 75–81. (d) Hao, L.; Gong, X.; Xuan, S.; Zhang, H.; Gong, X.; Jiang, W.; Chen, Z. *Appl. Surf. Sci.* **2006**, *252*, 8724–8733. (e) Arruebo, M.; Fernandez-Pacheco, R.; Irusta, S.; Arbiol, J.; Ibarra, M. R.; Santamaria, J. *Nanotechnology* **2006**, *17*, 4057–4064. (f) Li, Z. Z.; Wen, L. X.; Shao, L.; Chen, J. F. *J. Controlled Release* **2004**, *98*, 245–254.
(5) (a) Stoddart, J. F.; Colquhoun, H. M. *Tetrahedron* **2008**, *64*, 8231–8263. (b) Stoddart, J. F. *Chem. Soc. Rev.* **2009**, *38*, 1802–1820.

pore results only in the loss of the contents of that pore. In hollow particles with multiple pore connectivity to the hollow center, absence of control would result in the loss of all of the contents of the particles. In the work reported here, we demonstrate both superior loading of molecules and control by tunable pH-operable supramolecular nanovalves in which biologically relevant pH changes are used to trigger the release of guest molecules.

Hollow sphere silica materials with a mesoporous shell have been synthesized by using emulsions,[6] gas bubbles,[7] silica (or latex) beads,[8] and vesicles.[9] To make small (<200 nm) and uniformly sized hollow nanoparticles, we optimized a one-pot method that uses both polyvinylpyrrolidone (PVP-10) and dodecylamine (DDA) as co-templates.[10] Previous studies using only dodecylamine (DDA) as the template showed that conventional particles possessed a wormhole-like structure or sponge-like framework and amorphous morphology.[11] The hollow nanoparticles that result from the addition of PVP-10 also have wormlike pores with diameters of ∼2.7 nm. The large interior cavity makes them an intriguing candidate for drug loading and storage because of the possibility of a higher storage capacity than that of conventional mesoporous particles. However, little is known about control of the access to and from the interior. Sequential coating of hollow particles with cationic and anionic polymers offered some degree of control.[12] To explore direct gate-keeping control of pore openings, we designed a new and simple supramolecular nanovalve based on α-CD, a cyclic molecule that forms pH-dependent complexes with anili-noalkane stalks that are chemically bonded onto the silica surface.

Studies of host−guest complexation have shown that α-CD has a strong propensity for binding benzene and some of its derivatives.[13] The binding affinity between α-CD and the anilinoalkane group (Scheme 1) diminishes upon protonation of the aniline when the pH is lowered, causing the dissociation of the α-CD. A similar mechanism has employed the pH-dependent polypseudorotaxane formation between α-CD with

Scheme 1. Chemical Structures of the Linker Molecules
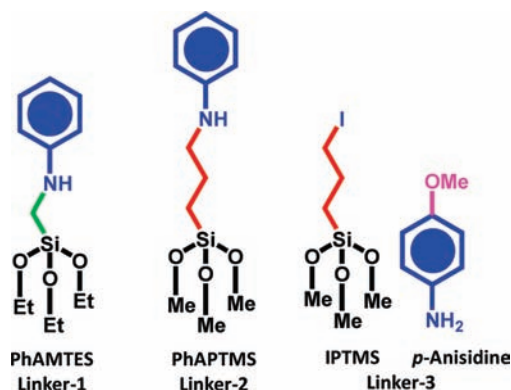
a triblock copolymer (PEI-*b*-PEG-*b*-PEI; PEG = poly (ethyl-eneglycol), PEI = polyethylene imine), where the α-CDs undergo reversible complexation (no charge on the nitrogens of PEI) and decomplexation (positive charge on the nitrogens of PEI) upon changes of pH.[14]

In this Article, we report studies of the abilities of three new and simple pH-responsive supramolecular nanovalves based on α-CD/aniline supramolecular systems (Figure 1) to control the pore openings on the surface of hollow nanoparticles and thus control the contents of the nanoparticles. The cargo capacity of the hollow particles is measured and compared to that of conventional mesoporous silica nanoparticles to determine if they encapsulate more guest molecules. Luminescence studies demonstrate that the release of cargo molecules occurs when the pH in the external medium is tuned down from neutral to acidic, and the anilinium nitrogen (on the stalk) is protonated. The ease of synthesis, straightforward operation, functional-versatility, and simplicity of design are key attributes of these new, pH-responsive mechanized nanoparticles.

Experimental Section

Experimental Materials. Distilled, deionized H$_2$O was obtained using a Millipore water purification system. Other analytical and reagent grade materials were used as purchased: tetraethoxysilane (TEOS) [98%, Aldrich], dodecylamine (DDA) [≥98%, Aldrich], polyvinylpyrrolidone (PVP-10) [≥98%, Aldrich], toluene (PhMe) [≥99.5%, EMD], methanol [99.9%, Fisher], triethylamine [99.5%, EMD], ethanol (EtOH) [200 proof, Pharmaco-AAPER], *N*-pheny-laminopropyltrimethoxysilane (PhAPTMS) [≥95%, Gelest], *N*-phenylaminomethyltriethoxysilane (PhAMTES) [≥95%, Gelest], 3-iodopropyltrimethoxysiliane (IPTMS) [≥95%, Gelest], *p*-anisidine [99%, Aldrich], propidium iodide (PI) [≥95%, Aldrich], Hoechst 33342 [≥97.0% (HPLC), Aldrich], and α-cyclodextrin (α-CD) [≥98%, Aldrich].

General Methods. Transmission electron microscope (TEM) images were collected on a JEM1200-EX (JEOL) instrument in the California NanoSystem Institute (CNSI). Powder X-ray dif-fraction (XRD) patterns were collected using a Philips X'Pert Pro diffractometer equipped with Cu Kα radiation. UV−vis spectra were collected using a Cary 5000 UV−vis−NIR spectrophotometer.

(6) (a) Sun, Q. Y.; Kooyman, P. J.; Grossmann, J. G.; Bomans, P. H. H.; Frederik, P. M.; Magusin, P. C. M. M.; Beelen, T. P. M.; Van Santen, R. A.; Sommerdijk, N. A. J. M. *Adv. Mater.* **2003**, *15*, 1097–1100. (b) Botterhuis, N. E.; Sun, Q. Y.; Magusin, P. C. M. M.; Van Santen, R. A.; Sommerdijk, N. A. J. M. *Chem.-Eur. J.* **2006**, *12*, 1448–1456. (c) Zhu, Y. F.; Shi, J. L.; Shen, W. H.; Chen, H. R.; Dong, X. P.; Ruan, M. L. *Nanotechnology* **2005**, *16*, 2633–2638. (d) Du, L.; Song, H. Y.; Yang, X.; Liao, S. J.; Petrik, L. *Microporous Mesoporous Mater.* **2008**, *113*, 261–267.

(7) (a) Rana, R. K.; Mastai, Y.; Gedanken, A. *Adv. Mater.* **2002**, *14*, 1414–1418. (b) Wang, J. G.; Li, F.; Zhou, H. J.; Sun, P. C.; Ding, D. T.; Chen, T. H. *Chem. Mater.* **2009**, *21*, 612–620.

(8) (a) Tan, B.; Rankin, S. E. *Langmuir* **2005**, *21*, 8180–8187. (b) Blas, H.; Save, M.; Pasetto, P.; Boissiere, C.; Sanchez, C.; Charleux, B. *Langmuir* **2008**, *24*, 13132–13137.

(9) (a) Yeh, Y.; Chen, B.; Lin, H.; Tang, C. *Langmuir* **2006**, *22*, 6–9. (b) Yu, M. H.; Wang, H. N.; Zhou, X. F.; Yuan, P.; Yu, C. Z. *J. Am. Chem. Soc.* **2007**, *129*, 14576–14577.

(10) Du, L.; Song, H. Y.; Liao, S. J. *Appl. Surf. Sci.* **2009**, *255* (23), 9365–9370.

(11) (a) Tanev, P. T.; Pinnavaia, T. J. *Science* **1995**, *267*, 865–867. (b) Tanev, P. T.; Pinnavaia, T. J. *Chem. Mater.* **1996**, *8*, 2068–2079. (c) Zhang, W.; Pauly, T. R.; Pinnavaia, T. J. *Chem. Mater.* **1997**, *9*, 2491–2498. (d) Pauly, T. R.; Liu, Y.; Pinnavaia, T. J.; Billinge, S. J. L.; Rieker, T. P. *J. Am. Chem. Soc.* **1999**, *121*, 8835–8842.

(12) (a) Zhu, Y.; Shi, J.; Shen, W.; Dong, X.; Feng, J.; Ruan, M.; Li, Y. *Angew. Chem., Int. Ed.* **2005**, *44*, 5083–5087. (b) Zhu, Y.; Shi, J. *Microporous Mesoporous Mater.* **2007**, *103*, 243–249. (c) Cai, W. Y.; Gentle, I. R.; Lu, G. Q.; Zhu, J. J.; Yu, A. M. *Anal. Chem.* **2008**, *80*, 5401–5406. (d) Yan, E. Y.; Ding, Y.; Chen, C. J.; Li, R. T.; Hu, Y.; Jiang, X. Q. *Chem. Commun.* **2009**, 2718–2720.

(13) (a) Liu, L.; Li, W. G.; Guo, Q. X. *J. Inclusion Phenom. Macrocyclic Chem.* **1999**, *34*, 291–298. (b) Golovanov, I. B.; Zhenodarova, S. M.; Tsygankova, I. G. *Russ. J. Gen. Chem.* **2006**, *76*, 267–271. (c) Chen, W.; Chang, C. E.; Gilson, M. K. *Biophys. J.* **2004**, *87*, 3035–3049. (d) Liu, L.; Li, X. S.; Song, K. S.; Guo, Q. X. *J. Mol. Struct. (THEOCHEM)* **2000**, *531*, 127–134. (e) Guo, Q. X.; Liu, L.; Cai, W. S.; Jiang, Y.; Liu, Y. C. *Chem. Phys. Lett.* **1998**, *290*, 514–518. (f) Liu, L.; Guo, Q. X. *J. Phys. Chem. B* **1999**, *103*, 3461–3467.

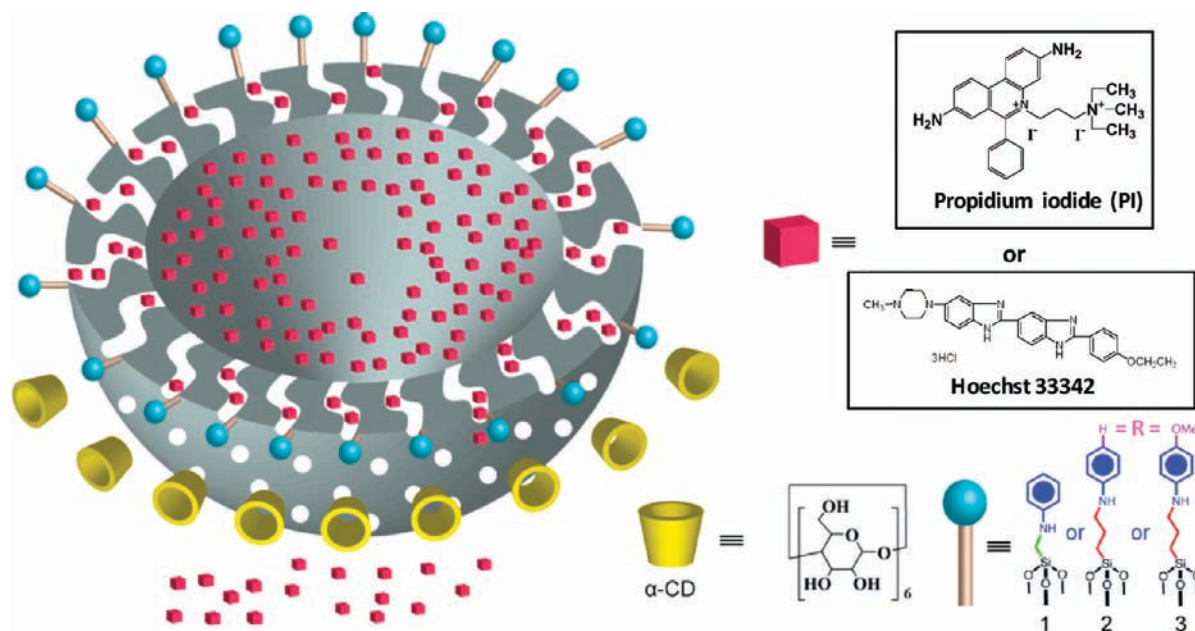(14) Park, C.; Oh, K.; Lee, S. C.; Kim, C. *Angew. Chem., Int. Ed.* **2007**, *46*, 1455–1457.

Figure 1. Depiction of a cross section of a hollow nanoparticle illustrating the wormlike pores connecting the interior to the surrounding solution. The stalks and the α-CD rings that control the pore openings are also shown.

The controlled release profiles were obtained via luminescence spectroscopy using an Acton SpectraPro 2300i CCD and a coherent Argon Innova 90C-5-excitation laser. Dynamic light scattering was performed on a Beckman Coulter N4 Plus particle sizer, with a 633 nm HeNe excitation source. The measurements were carried out in EtOH on extracted hollow nanoparticles prior to any surface modifications. N_2 adsorption−desorption isotherms were obtained at 77 K on a Micromeritics ASAP2020 automated sorption analyzer. The BET model was applied to evaluate the specific surface areas. Pore size and pore volume were determined from the adsorption data by BJH method. All solid-state NMR experiments were performed on dry powder samples using a Bruker DSX-300 MHz spectrometer and with a 4 mm double resonance Bruker probe head. Zirconium oxide 4 mm rotors were used with Kel-F caps for all measurements. Thermal stability measurements were collected on a Pyris Diamond TG/DTA (Perkin-Elmer Instruments) between 100 and 900 °C with a heating rate of 20 °C/min.

Preparation of Hollow and Conventional Mesoporous Silica Nanoparticles. Hollow mesoporous silica particles were synthesized by using DDA as the main template, and PVP-10 (MW ≈ 10 000 g/mol) as the cotemplate. PVP (0.5 g) was dissolved in a EtOH/H_2O mixture (2.5:8 v/v) with 60 min of stirring. DDA (1.3 g) was then added into the solution, and after 30 min of stirring, TEOS (5 mL) was added, and the mixture was stirred at room temperature for 24 h. The final product was precipitated, filtered, and then dried under vacuum. Removal of both templates (DDA and PVP-10) was achieved by solvent extraction: silica particles (1.0 g) were suspended in EtOH (100 mL), and the mixture was heated under reflux for 24 h. The solvent-extracted particles were washed extensively with EtOH and collected via vacuum filtration.

Conventional mesoporous silica nanoparticles were synthesized with the same procedure as that used for the hollow particles, except that the concentration of the PVP-10 templates (0.1 g) was lowered.

Construction of Supramolecular Nanovalves (SNV). Three versions of supramolecular nanovalves were synthesized: (1) SNV-1, *N*-phenylaminomethyltriethoxysilane (PhAMTES) as the linker-1 molecule, (2) SNV-2, *N*-phenylaminopropyltrimethoxysilane (PhAP-TMS) as the linker-2 molecule, and (3) SNV-3, 3-iodopropyltri-methoxysilane (IPTMS), and *p*-anisidine as the linker-3 molecules, as shown in Scheme 1.

To achieve an anilinoalkane-functionalized silica surface, mesoporous silica nanoparticles (100 mg of hollow or conventional particles) were treated with linker molecules (0.1 mmol of PhA-MTES or PhAPTMS) in dried PhMe (10 mL) and allowed to reflux under N_2 for 24 h. For the SNV-3 system, nanoparticles with linker-3 were derivatized first with IPTMS (0.1 mmol) in dried PhMe for 24 h refluxing, filtered, then washed thoroughly with PhMe and MeOH, and dried in a vacuum oven. Next, *p*-anisidine (1.0 mmol) and triethylamine (3.0 mmol, as catalyst) were added to the IPTMS-functionalized particles in toluene solution, and the reaction mixture was heated under N_2 at reflux for another 2 days. The anilinoalkane-functionalized materials were then collected using vacuum filtration, followed by additional washing with toluene and MeOH, prior to drying in vacuum. Cargo molecules, propidium iodide (PI, 1 mM aqueous solution) or Hoechst 33342 (1 mM aqueous solution), were loaded into the nanopores by diffusion for 24 h at room temperature. Finally, the PI or Hoechst 33342-loaded, anilinoalkane-functionalized nanoparticles were capped with α-CD (0.2 g). The resulting mixture was stirred for 3 days at room temperature prior to further washing, filtering, and drying under vacuum.

Controlled Release Experiments. A sample of PI-loaded, α-CD-capped SNV (4 mg) was placed in the corner of a cuvette. Distilled H_2O (6 mL) was carefully added (pH ~7) into the cuvette to avoid agitating or disarranging the nanoparticles. The emission of PI in the solution above the particles was measured as a function of time by using a 448 nm excitation beam (10 mW) to excite the dye molecules as they are released from the nanopores. The PI emission spectrum was recorded as a function of time at 1 s intervals. Release profiles were obtained by plotting luminescence intensities of PI at the emission maximum (650 nm) as a function of time. Activation of the nanovalves was accomplished by adjusting the pH of the solution to the range of ~3.5 to ~6 with addition of HCl solution (0.1 M). The solution was gently stirred in the cuvette throughout all controlled release experiments.

The release profiles of Hoechst 33342 were recorded by the same procedure as that used for the PI-loaded SNV nanoparticles, except that 377 nm was used as the excitation beam and luminescence
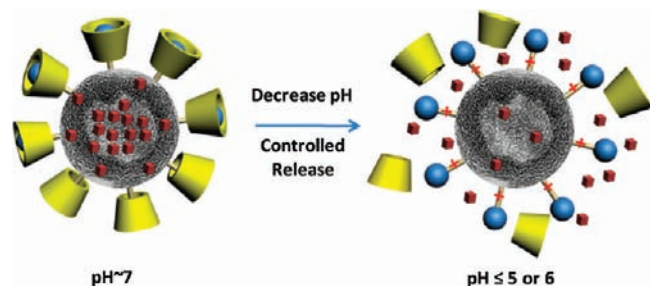
Figure 2. At pH ~7, the aniline nitrogens on the stalks are not protonated and are encircled by the α-CD rings that block the pores (left). Upon decreasing the pH, protonation of the nitrogen causes α-CD to dissociate, unblocking the pores and releasing the trapped cargo molecules from the interior (right).

intensities of Hoechst 33342 were collected at its emission maximum (500 nm) as a function of time.

Results and Discussion

1. Design and Synthesis of Mechanized Hollow and Conventional Particles. The hollow and conventional particles were prepared through a facile one-pot sol−gel process involving the use of DDA and PVP as the cotemplates, and TEOS as the silica precursor. The assembly of the supramolecular nanovalves on the dye-loaded nanoparticles was carried out in a stepwise process from the nanoparticle surface outward. Briefly, beginning with the as-synthesized nanoparticles, the DDA and PVP templates were removed by EtOH extraction to generate empty, accessible nanopores. Next, one of the three supramolecular nanovalves (SNV) with different linkers was attached to the silica surface through treatment with *N*-phenylaminomethyltriethoxysilane (PhAMTES, denoted linker-1), *N*-phenylaminopropyltrimethoxysilane (PhAPTMS, denoted linker-2), or 3-iodopropyltrimethoxy-siliane (IPTMS and *p*-anisidine, denoted linker-3). The cavities of the linker-functionalized hollow nanoparticles were then loaded with fluorescent PI or Hoechst 33342, cargo molecules. Finally, α-CD was added as the capping agent to gate the entrance of the nanopores. A cross section of a hollow SNV system, the chemical structures of the components, and the cargo are shown in Figure 1. The operation of SNV systems depends on α-CD rings that encircle anilinoalkane stalks, which, upon protonation, release the α-CD rings and enable the encapsulated guest molecules to escape into solution as shown in Figure 2.

Optimization of the system requires choosing a proper linker length. If the linker were too long, then the α-CD cap would be too far from the pore to block it efficiently, resulting in a leaky system. However, if the linker is too short, then α-CD could not interact strongly with the stalk, and the system would not be formed. In our studies, two linker lengths were tested: PhAMTES, where the amine group is one carbon atom away from silica, and PhAPTMS, where the amine group is separated by three carbons.[15]

2. Properties of the Nanoparticles. Mesoporosities of both hollow and conventional particles were verified using powder X-ray diffraction (Supporting Information Figure S1). Lattice spacing for both types of particles was ~3.97 nm. The sizes of the hollow particles and its hollow cavity were evaluated using transmission electron microscopy (TEM) as shown in Figure 3a,b. Hollow particles have an average diameter of 100 nm in
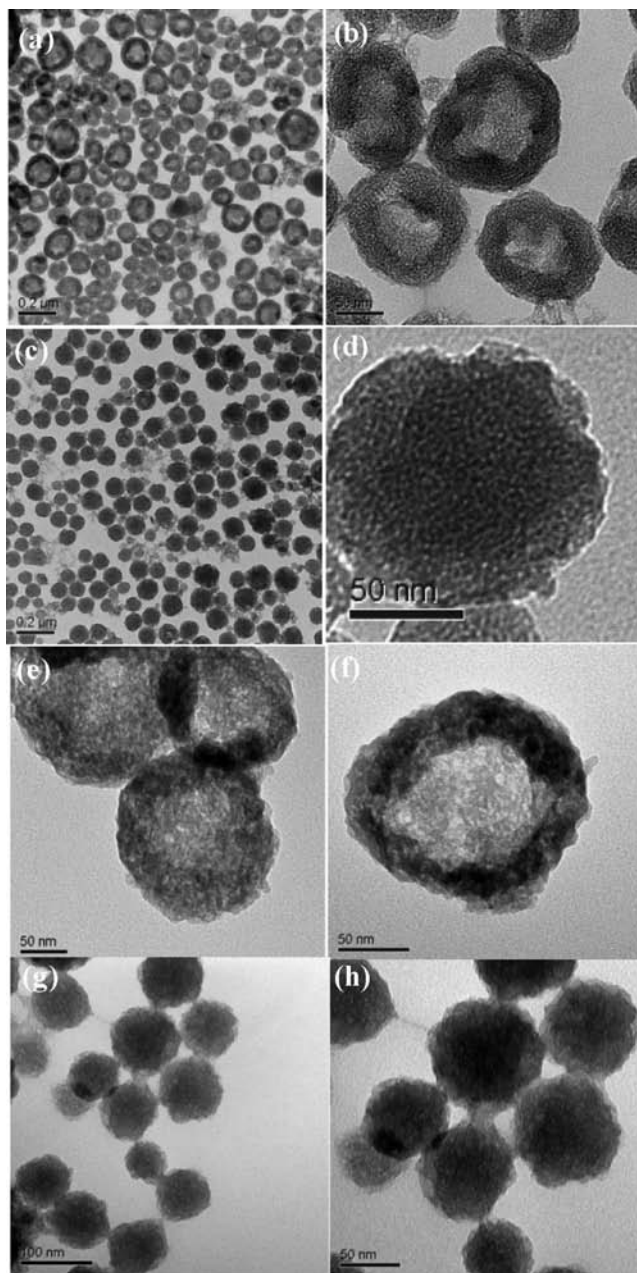
(15) Nguyen, T. D.; Liu, Y.; Saha, S.; Leung, K. C. F.; Stoddart, J. F.; Zink, J. I. *J. Am. Chem. Soc.* **2007**, *129*, 626–634.

Figure 3. TEM images of hollow (a,b,e,f) and conventional (c,d,g,h) nanoparticles. Unfunctionalized particles are shown in (a)−(d), and particles loaded with PI and capped by α-CD are also shown (e−h). The wormlike pore structure is most clearly seen in (b) and (d).

the TEM images, and the transparency of these particles confirmed its hollow core characteristics. Furthermore, the TEM images (Figure 3b and d) showed that both the hollow and the conventional particles have a worm-like structure, unlike the ordered hexagonal pore structure of MCM-41. It should be noted in Figure 3e−h that both the hollow and the conventional SNV particles exhibit a less clear pore structure because these particles are cargo-loaded and capped with α-CD.

From N_2 adsorption data obtained at 77 K (Supporting Information Figure S2), the pore sizes of the hollow and conventional particles are determined to be 2.74 and 2.69 nm, respectively, as shown in Table 1. In addition, the evolution of the porosity with the inclusion of the functionalization of the mesopore outlets can be calculated from the isotherms (Sup-

Table 1. Properties of Hollow and Conventional Particles Calculated from N_2 Adsorption−Desorption Isotherms

sample	S_{BET} [m² g⁻¹]	BJH pore size[a] [nm]	V_t[b] [cm³ g⁻¹]	V_f[c] [cm³ g⁻¹]	V_{tx}[d] [cm³ g⁻¹]
hollow particles	1006	2.74	1.377	1.079	0.298
hollow particles with linker-2	998	2.65	1.030	0.752	0.278
hollow particles with linker-2 and α-CD	986	2.62	0.895	0.667	0.228
conventional particles	924	2.69	1.043	0.985	0.058

[a] Pore size estimated by using the BJH model applied on the adsorption branch of the isotherm. [b] V_t, total pore volume according to the BJH adsorption cumulative volume of pores between 1.7000 and 300.0000 nm diameter. [c] V_f, framework volume obtained from the volume of pores between 1.7000 and 5.0000 nm diameter, which can be associated with the surfactant generated mesopores. [d] V_{tx}, textural pore volume obtained from the difference ($V_t - V_f$), interpreted as a combination of both large inner-core macropores and cavities formed when more than one particle is fused together.

porting Information Figure S2). In contrast with unfunctionalized hollow particles, very similar pore sizes have been determined: 2.65 nm for linker-2 functionalized hollow particles and 2.62 nm for α-CD capped hollow particles with linker-2. These values suggest that the linker molecules exist predominantly at the exterior surface of the particles rather than at the interior surface of the pore channels. In addition, N_2 adsorption−desorption isotherms (Supporting Information Figure S2) also substantiate the hypothesis that hollow particles could load more cargo molecules inside its cavity than could conventional particles, because hollow particles have a bigger pore volume (1.377 cm³ g⁻¹) than do conventional particles (1.043 cm³ g⁻¹) as shown in Table 1. The textural pore volume of conventional particles is 0.058 cm³ g⁻¹. However, the textural pore volume of hollow particles is 0.298 cm³ g⁻¹, which is bigger than that for conventional particles. It is interpreted as the sum of the volumes of both large inner-core macropores and cavities formed when more than one particle is fused together. The total pore volumes of the hollow particles show a decrease after each functionalization step. When the hollow particles are functionalized with linker-2 molecules, V_t decreases to 1.030 cm³ g⁻¹. While the hollow particles with linkers are capped with α-CD, V_t further decreases to 0.895 cm³ g⁻¹; the value may indicate that α-CD may offer some degree of blocking of the pore openings to a molecule as small as N_2.

^{13}C CP/MAS SSNMR of linkers -1, -2, and -3 on hollow particles and of unfunctionalized hollow particles were obtained (Supporting Information Figure S3). The unfunctionalized hollow particles (Figure S3a) have three peaks in the aliphatic region that are attributed to reaction of free alcohol (MeOH and EtOH), formed by the condensation reaction, with surface silanol groups.[16] The ^{13}C CP/MAS SSNMR spectrum for linker-3 shows four peaks in the aliphatic region from the propyl and methoxy groups and four benzyl peaks in the aromatic region (Figure S3b). Similarly, linker-1 has one peak in the aliphatic region from the methylene carbon atoms and four benzyl peaks in the aromatic region of the ^{13}C CP/MAS SSNMR spectrum (Figure S3c). Last, the ^{13}C CP/MAS SSNMR spectrum of linker-2 has three peaks in the aliphatic region from the propyl chain and four benzyl peaks in the aromatic region (Figure S3d).

^{29}Si CP/MAS SSNMR was also used to characterize linkers -1, -2, and -3, the precursor to linker-3 (IPTMS), and unfunctionalized hollow particles (Supporting Information Figure S4). The unfunctionalized particles show three peaks in the Q region of the ^{29}Si CP/MAS SSNMR spectrum, attributed to the silicon atoms in the bulk silica. The ^{29}Si CP/MAS SSNMR spectra of linkers -1, -2, -3, and IPTMS show peaks in the T and Q regions

(Figure S4e, d, c, and b, respectively), which are attributed to the silicon atoms in the bulk silica (Q region) and the silicon atoms from the respective immobilized molecules (T region).[17]

The thermal behavior of the hollow particles was explored by thermogravimetric analysis (TGA) in air (Supporting Information Figure S5). The weight loss of pure hollow particles (~5 wt %, Figure S5a) is not a result of incompletely removed template molecules but rather could be attributed to the combustion of ethoxy groups generated by esterification of the silanol surface during the extraction procedure.[18] According to the TGA curves, the decomposition of linker-2, the capping agent (α-CD), and the cargo (PI) molecules takes place between the temperatures of 100−700 °C. An additional weight loss can also be observed for each further functionalization step. When hollow particles were functionalized with linker molecules, α-CD, and PI molecules, respectively, the relevant total weight loss was ~12 wt % (Figure S5b), ~20 wt % (Figure S5c), and ~29 wt % (Figure S5d).

Multiple studies have shown that mesoporous silica nanoparticles are noncytotoxic and undergo cellular uptake into acidic lysosomes through endocytosis.[19] For endocytosis to take place, small particle is crucial. The size of the hollow particles suspended in EtOH was probed using dynamic light scattering (DLS, Supporting Information Table S1). The average particle size was ~278 nm in diameter, which is small enough to be taken up by cells.

3. Operation of the SNV Systems. The operation of the pH-responsive hollow SNV particles was monitored in aqueous solution using luminescence spectroscopy. Figures 4 and 5 depict release profiles of PI and Hoechst 33342 from the SNV systems, respectively. The emission intensity of both PI and Hoechst 33342 before any triggered release was monitored for ~30 min. The flat baselines show that leakages from both systems are negligible. Next, the pH of the system was decreased from ~7 to ~3.5 by the addition of 0.1 M HCl. The emission intensities of both PI and Hoechst 33342 in solution increase rapidly, confirming that the α-CD rings unblock the pore openings and allow the contents to escape into solution. The similarity between release profiles of both PI and Hoechst 33342 from the SNV-1 and SNV-2 systems suggests that both linkers are equally compatible with α-CD such that negligible leakage of both PI and Hoechst 33342 occurs prior to acid activation of the nanovalves. The release profiles (Figures 4c and 5c)

(16) Bluemel, J. *J. Am. Chem. Soc.* **1995**, *117*, 2112–2113.

(17) Peng, C.; Zhang, H.; Yu, J.; Meng, Q.; Fu, L.; Li, H.; Sun, L.; Guo, X. *J. Phys. Chem. B* **2005**, *109*, 15278–15287.

(18) (a) Kecht, J.; Bein, T. *Microporous Mesoporous Mater.* **2008**, *116*, 123–130. (b) Kecht, J.; Schlossbauer, A.; Bein, T. *Chem. Mater.* **2008**, *20*, 7207–7214.

(19) (a) Lu, J.; Liong, M.; Sherman, S.; Xia, T.; Kovochich, M.; Nel, A. E.; Zink, J. I. *Nanobiotechnology* **2007**, *3*, 89–95. (b) Lin, Y. S.; Wu, S. H.; Hung, Y.; Chou, Y. H.; Chang, C.; Lin, M. L.; Tsai, C. P.; Mou, C. Y. *Chem. Mater.* **2006**, *18*, 5170–5172.
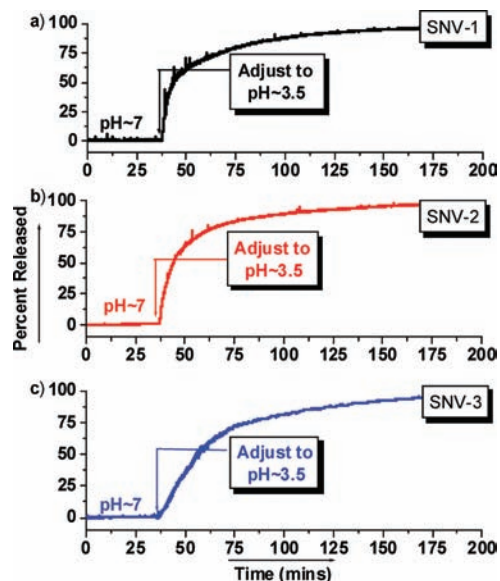
Figure 4. Release profiles of PI from hollow supramolecular nanovalve (SNV) systems with linkers 1−3 (top to bottom). Luminescence spectroscopy was used to monitor PI as it was released into the solution. Negligible leakage was observed for all systems prior to acidification. The amount of cargo released after acidification increases rapidly and then asymptotically approaches its maximum.
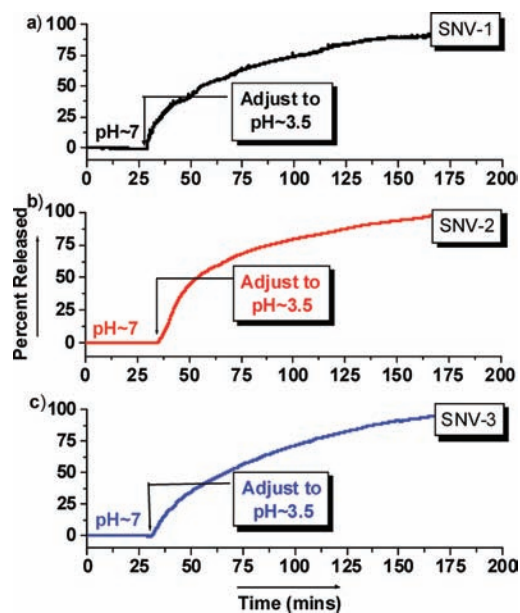

Figure 5. Release profiles of Hoechst 33342 from hollow supramolecular nanovalve (SNV) systems with linkers 1−3 (top to bottom). Luminescence spectroscopy was used to monitor Hoechst 33342 as it was released into the solution. Negligible leakage was observed for all systems prior to acidification. The amount of cargo released after acidification increases rapidly and then asymptotically approaches its maximum.

demonstrate that the cargo release capability of the pH-responsive SNV-3 system is similar to that of SNV-2 at pH ∼3.5 when the phenyl group is substituted (R = OMe). As a control experiment, the cargo release of the pH-responsive SNV-2 system was tested in the absence of α-CD. As shown in the release profile in the Supporting Information (Figure S6), a sustained release could be witnessed (Figure S6a) if the PI-loaded hollow particles were not washed. However, when PI-loaded hollow particles were washed thoroughly, as expected,
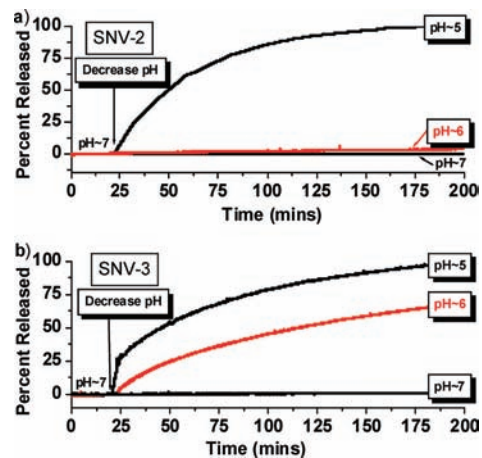

Figure 6. pH dependence of the release profiles of PI from hollow SNV-2 (a) and SNV-3 (b) systems. Both systems retain cargo molecules at pH ∼7. Cargo release at pH ∼6 is small when R = H in the SNV-2 system but is fast when R = OMe in the SNV-3 system.
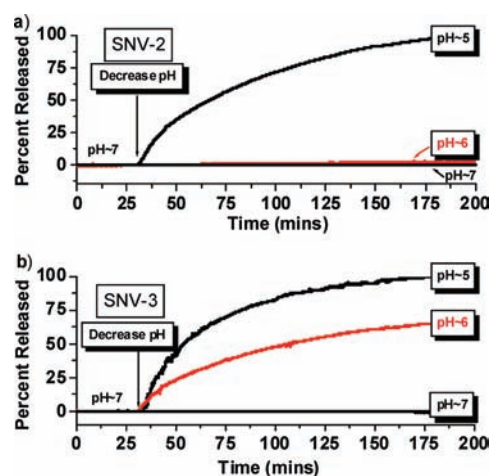

Figure 7. pH dependence of the release profiles of Hoechst 33342 from hollow SNV-2 (a) and SNV-3 (b) systems. Both systems retain cargo molecules at pH ∼7. Cargo release at pH ∼6 is small when R = H in the SNV-2 system but is fast when R = OMe in the SNV-3 system.

Table 2. Weight Percentages of PI and Hoechst 33342 Released from SNV Particles

	hollow particles		conventional particles	
nanovalves	PI/particle wt %	Hoechst 33342 / particle wt %	PI/particle wt %	Hoechst 33342 / particle wt %
SNV-1	4.82	3.30	2.31	1.69
SNV-2	3.45	2.45	1.70	1.30
SNV-3	3.22	2.01	1.43	0.99

no PI was released after the lowering of the pH because the cargo molecules had escaped from the unguarded pores when the particles were washed before testing (Figure S6b).

Tuning of the pH at which the valves open into a biologically relevant range is possible by changing the substituents on the phenyl ring. When the external pH drops below the pK_a value of the aniline nitrogen, the noncovalent interactions decrease and the α-CD dissociates. The pK_a of p-anisidine ($pK_a \approx 6$) is approximately 1 pK_a unit more basic than that of aniline ($pK_a \approx 5$). The effects of different pH's on the release profiles for R = H and −OMe are shown in Figures 6 and 7. There is
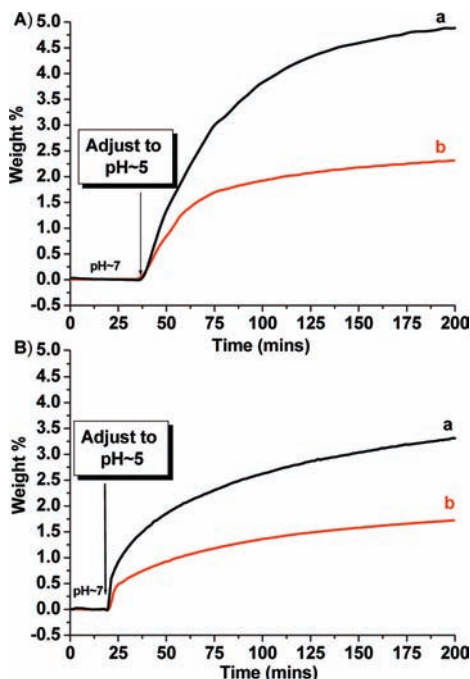
Figure 8. Weight percent release profiles of PI (top) and Hoechst 33342 (bottom) using the SNV-1 system. Releases from the hollow particles are shown by curves a and from conventional particles by curves b.

negligible leakage for 200 min from either system at pH = 7. When the pH is adjusted to ~5, the aniline nitrogen on linker-2 is protonated and the valve opens (Figures 6a and 7a). However, when the pH is tuned to ~6, the system is not significantly activated. In contrast, when R = OMe, significant activation at pH ~6 is observed. The time required to achieve 50% release of the cargo at pH ~5 is about the same for both R = OMe and R = H (about 30 min), while at pH ~6, the time required is about 100 min for R = OMe, but the release is negligible from the R = H system even after 5 h.

4. Efficiency of the SNV Systems in Relation to Different Silica Particles. Finally, we investigated the loading capacity of the hollow and conventional silica particle nanovalve systems. Efficiency is quantified by the amount of PI or Hoechst 33342 that is released per particle mass. The amount of PI or Hoechst 33342 released is measured by taking the supernatant's absorbance (6 mL) before and after the luminescence spectroscopy experiments. The absorption spectra of PI and Hoechst 33342 in H₂O before (pH ~7) and after (pH ~5) the release are shown as Figures S7, S8 in the Supporting Information.

Absorbance measurements of both 0.1 mM (pH ~5) of PI and 0.01 mM (pH ~5) of Hoechst 33342 are used as the standard (Supporting Information Figures S7A, S8A), and weight percentages of both PI and Hoechst 33342 are calculated

on the basis of the 492 nm (PI) and 347 nm (Hoechst 33342) absorption peak (Supporting Information Figures S7B,C and S8B,C, respectively). The release profiles expressed in weight percentages of both PI and Hoechst 33342 from SNV-1 nanosystems using hollow and conventional particles are shown in Figure 8A and B, respectively. Additionally, the calculated weight percentages of all three systems (SNV-1, SNV-2, and SNV-3) are given in Table 2.

Two observations contained in Table 2 and Figure 8 are important to highlight. First, the hollow particles are capable of storing and subsequently releasing twice as much cargo material as the conventional particles. Second, a consistent trend is observed that nanovalves functionalized with shorter linkers (length of linker-1 is the shortest, while linker-3 is the longest) can load more PI molecules. This trend could be partly explained through the fact that the methoxy substituent group on linker-3 has increased the molecule's hydrophobicity. Because both cargo molecules are water-soluble and hydrophilic, the hydrophobic group on the linker makes it energetically less favorable for some of the dye molecules to go inside the pores.

Summary

Three permutations of new pH-responsive supramolecular nanovalves were tested on both hollow and conventional mesoporous silicas. They were opened by decreasing the pH of the surrounding solution. Luminescence spectroscopy was used to demonstrate that these supramolecular nanovalves encapsulated both PI and Hoechst 33342 molecules at neutral pH, and to measure the rate of the release under acidic stimulation. The pH at which the valves open was tuned by changing the substituents on the stalk. Importantly, no leakage was observed in H₂O solution before the pH was decreased. These studies showed that hollow mesoporous nanoparticles release as much as 2 times more cargo molecules than do conventional mesoporous nanoparticles. Efforts are now underway to explore the applications of these nanovalves by testing their delivery capabilities in different types of human cancer cells.

Supporting Information Available: Powder XRD patterns, N₂ adsorption−desorption isotherms, pore size distributions, ¹³C CP/MAS SSNMR, ²⁹Si CP/MAS SSNMR, TGA, tabulated DLS, luminescence spectra, and UV−vis spectra. This material is available free of charge via the Internet at http://pubs.acs.org.

JA904982J